An electrochemical paper-based hydrogel immunosensor to monitor serum cytokine for predicting the severity of COVID-19 patients

Dongmin Shi [a,b,*], Chiye Zhang [a], Xiaoyuan Li [c], Jie Yuan [a]

[a] *Department of Electronic & Computer Engineering, The Hong Kong University of Science and Technology, Hong Kong Special Administrative Region of China*
[b] *Individualized Interdisciplinary Program (Microelectronics), The Hong Kong University of Science and Technology, Hong Kong Special Administrative Region of China*
[c] *Department of Chemistry, The Hong Kong University of Science and Technology, Hong Kong Special Administrative Region of China*

ABSTRACT

Analysis of cytokines levels in human serum is critical as it can be a "symptom diagnostic biomarker" in COVID-19, giving real-time information about human health status. Here, we present the construction and performance of a low-price immunosensor (~US$0.428 per test) based on microfluidic paper-based system to detect cytokine for predicting the health status of COVID-19 patients. Interleukin-6 (IL-6) was selected as the detection model for the close relationship between IL-6 and COVID-19. The assay, which we integrated into foldable paper system, leverages the magnetic immunoassay, the streptavidin-horseradish peroxidase (HRP) associated with tetramethyl benzidine/hydrogen peroxide (TMB/H_2O_2) to amplify the signal for electrochemical readout. To improve the sensitivity of cytokine detection, a hybrid of gold nanoparticles (AuNPs) and polypyrrole (PPy) hydrogel was modified on the working electrode to increase the conductivity and improve the electron transfer rate. With our prototypic origami paper-based immunosensor operated in differential pulse voltammetry (DPV) mode, we achieved excellent results with a dynamic range from 5 to 1000 pg/mL and a lower detection limit (LOD) of 0.654 pg/mL. Furthermore, we evaluated the capability of the clinical application of the proposed immunosensor using human serum samples from a hospital. The results indicate that our proposed immunosensor has great potential in early diagnosing high-risk COVID-19 patients.

1. Introduction

A novel coronavirus disease 2019 (COVID-19) resulting from severe acute respiratory syndrome coronavirus 2 (SARS-CoV-2), first emerged in Wuhan, China, and quickly evolved into a worldwide viral pandemic (Andersen et al., 2020; Wu et al., 2020). By April 2022, more than 507 million people worldwide had fallen ill with the virus and the death toll had reached 6.21 million. Although patients with COVID-19 may have asymptomatic clinical manifestations, others have mild upper respiratory symptoms or progress to severe pneumonia and even acute respiratory distress syndrome (ARDS) (Broughton et al., 2020; Cazzolla et al., 2020). Current efforts to identify infected people mainly lie in nucleic acid testing based on reverse transcription-polymerase chain reaction (RT-PCR). However, the detection of severity predictors for infected individuals has been halted. Severe symptoms are accompanied by an aggressive inflammatory cytokine storm (Tetro, 2020; Yang et al., 2020). Interleukin-6 (IL-6) plays a pivotal function in the cytokine storm by activating a variety of acute-phase proteins. The aberrant expression of IL-6 has been found in the serum of patients with severe clinical manifestations (Chen et al., 2020; Maucourant et al., 2020; Tanaka et al., 2014; Tetro, 2020). Hence, close monitoring of cytokine, especially IL-6, is of utmost importance to predict the severity of COVID-19 patients and focus the treatment efforts on patients to reduce the mortality rate and improve survival rates.

The current standard workhorse assay to test cytokines in the blood is the well-known enzyme-linked immunosorbent assay (ELISA) (Gao et al., 2021; Indalao et al., 2017). However, the natural levels of cytokines under physiological conditions are very low (~pM range) (Noh et al., 2022). In addition, due to the synergistic interaction between different cytokines, one cytokine can affect neighbored cytokines secretion and expression, which makes the cytokine network complicated (Stenken and Poschenrieder, 2015). Furthermore, economic factors limit intensive treatment in some poverty-stricken areas due to the shortage of adequately equipped laboratories. These challenges greatly limit the traditional techniques for measuring cytokines during this pandemic. Other alternatives based on traditional techniques, such as

---

fluorescence spectroscopy (Toma and Tawa, 2016), colorimetry (Peng et al., 2016) and radioimmunoassay (Peppard et al., 1992), still suffer from one or more of the following drawbacks: bulky equipment, the requirement of huge sample volume, high cost, and low sensitivity. Consequently, there is a push to implement devices for monitoring cytokines throughout a broad dynamic range with high potency, low cost and high sensitivity.

The microfluidic system has been raised as an alternative for the detection of cytokines since its prominent features include controllable sample handling, low reagent consumption, shorter analysis time and excellent analytical performance (Mou and Jiang, 2017; Nge et al., 2013; Song et al., 2019). However, many microfluidic devices are still confined to laboratories due to the need for extra pumps and valves. With the goal of reducing costs and increasing mobility, microfluidic paper-based analytical devices (μPADs) were developed. Whitesides et al. proposed μPADs for the first time in 2007, and they have since raised considerable interest with the benefits of simplicity, portability, competitive price, favorable biocompatibility and capillary-driven features (Martinez et al., 2007; Santhiago et al., 2013). To date, researchers have integrated various chemical approaches (colorimetry, fluorometry, electrochemistry, *etc.*) with paper to construct microfluidic devices for quantitative and multiplex analyses in many fields (Naseri et al., 2020; Qi et al., 2018; Tenda et al., 2018), especially in the detection of COVID-19 (de Lima et al., 2021; Torrente-Rodríguez et al., 2020; Torres et al., 2021; Zhang et al., 2022).

Conductive polymer hydrogels (CPHs) show great potential for applications in bioelectronics devices owing to their excellent features, including a high surface-to-volume ratio, superior conductivity and outstanding biocompatibility. (Wang et al., 2019; Zhai et al., 2013). The nanoparticles dispersed in conductive hydrogel are an efficient way to improve biosensor properties. Several teams have recently reported hydrogel sensors for detection biomolecules or proteins. (Li et al., 2015; Liang et al., 2020; Yang et al., 2021). Remarkable achievements have been made in biological detection using a hydrogel constructed biosensor. However, bio-sensing platforms for cytokines detection based on conductive hydrogels and noble nanoparticles are rarely reported.

We report for the first time a new device that integrates AuNPs and PPy hydrogel with an origami microfluidic paper-based electrochemical immunosensor (AuNPs/PPy/o-μPEIS). This device was used to detect cytokine leveraging fast-response differential pulse voltammetry (DPV). The o-μPEIS was prepared based on wax printing and the screen-printed technique was used to fabricate the electrodes. The network nanostructure of PPy hydrogel played a dominant role in the deposition of AuNPs. Not only did it function as a platform for immobilized biomolecules, but it also provided a 3D channel for efficient electron transport. AuNPs were embedded with PPy hydrogel as the sensing interface, increasing the sensitivity significantly by increasing the surface area and conductivity of the sensor. This paper-based immunosensor utilizes magnetic beads for immunomagnetic enrichment and signal amplification. As an enzyme label, HRP was integrated into this sensor. IL-6 was chosen as the model target. The strengths of this proposed immunosensor include: (1) compared to traditional immunosensor, this proposed device could provide high sensitivity with low cost and low sample consumption; (2) compared to other paper-based devices, this device is easier to operate and preferable for non-professionals to use. This origami microfluidic paper-based device offers a possibility of detecting cytokine for effective evaluation of the health status of COVID-19 patients. Fig. 1 presents the principle of this AuNPs/PPy/o-μPEIS for the detection of IL-6, the details are described in the following section.

2. Experimental section

2.1. Chemicals and apparatus

All chemicals, apparatus and details of synthesis of PPy hydrogel are provided in Supporting Information.

2.2. Design and fabrication of o-μPEIS

Our microfluidic paper-based sensor is shown in Fig. 2A, Whatman No. 1 chromatography paper was utilized as a substrate. White areas are hydrophilic, whereas all other color zones have hydrophobic surfaces. There are three tabs on this device. Tab 1 is a microfluidic channel tab to introduce the sample inlet. The capillary force will propel the sample flow through the microfluidic channel and reach the surface of the working electrode (WE). To cut costs and save space, two chambers, namely a reaction chamber and a detection chamber, were placed on one tab. The diameter of each chamber is 5 mm. Immunological discrimination occurs in the reaction chamber, whereas enzyme catalytic reactions occur in the detection chamber. A WE of 3 mm in diameter was situated in the purple region and served as a detecting tab (tab 2). The reference electrode (RE) and the counter electrode (CE) were grouped in a white hole (7 mm in diameter) and printed on the opposite side of the auxiliary tab (tab 3). It is essential to separate the WE and auxiliary electrodes to avoid contamination during incubation.
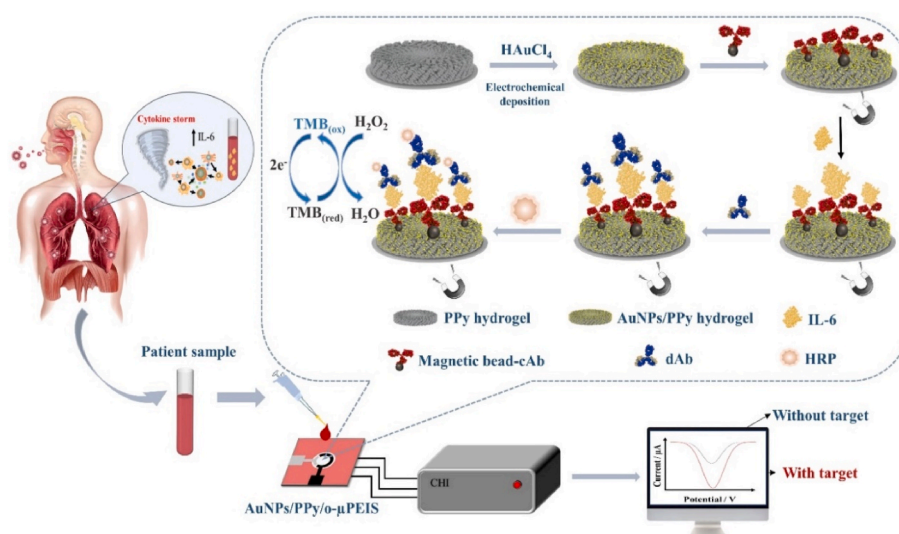
Fig. 1. Schematic representation of the o-μPEIS for detecting of IL-6 based on hybrid of AuNPs and PPy hydrogel. The HRP/TMB/H$_2$O$_2$ system was applied to generate the electrochemical signal readout to verify the detection principle.
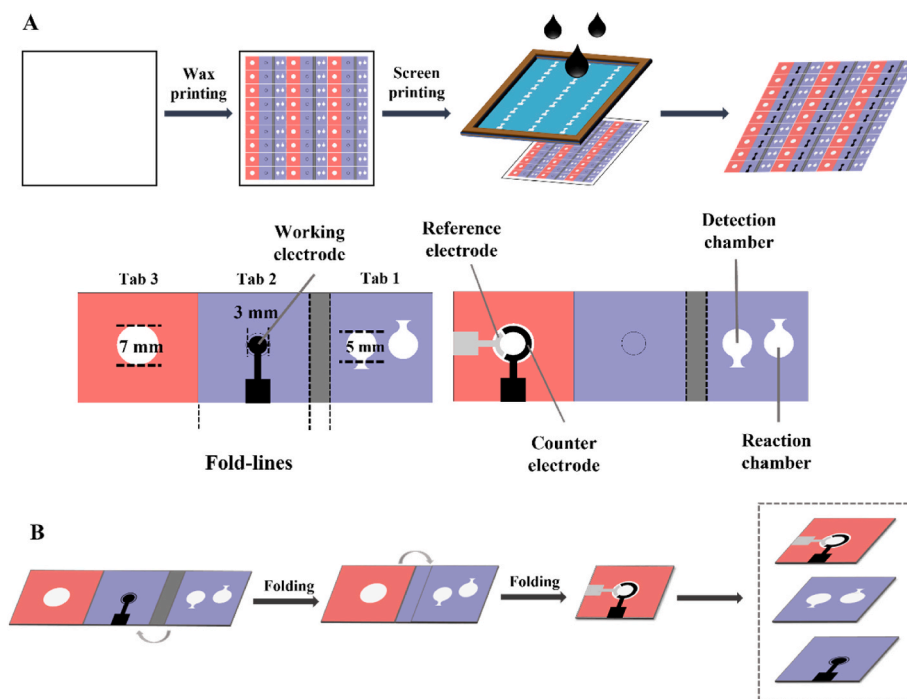
Fig. 2. Overview of the origami microfluidic paper-based electrochemical immunosensor. (A) Schematic illustration of the fabrication procedure and structure of o-μPEIS. The o-μPEIS was prepared and used in three steps: (1) constructing hydrophilic areas by wax printing, (2) printing layer of carbon ink and silver ink to the paper to fabricate electrodes, (3) baking in an oven to dry the electrodes. (B) The folding process of the proposed o-μPEIS: fold tab 1 to tab 2, following fold tab 3.

The three solid lines define the fold-line. By folding along folding lines, the reaction chamber and detection chamber was able to be aligned with the WE on the detection tab. Continuing folding along line 3, the three electrodes were able to connect once the fluid filled the white hole. This device shows unique advantages in sensor operation, manufacturing cost, and detection performance thanks to origami technology.

The following is a description of the manufacturing procedure for this sensor, which does not need specialized equipment or an experimental environment. First, we designed the shape and structure of our sensor. The overall size of this sensor is 20 mm × 60 mm with three tabs. Then, we patterned hydrophobic illustrations on paper using Xerox digital wax printer (Fig. S1), followed by baking in an oven at 110 °C for 4 min. Due to the unique porous nature of paper, the printed wax melted and permeated the material (Fig. S2). The unprinted portion retained the paper's favorable characteristics, such as high hydrophilicity. The screen-printed electrodes were then fabricated using a DEK260 stencil printer (Fig. S3). The WE and CE were made of carbon ink, the RE was made of Ag/AgCl ink. Finally, after being folded as shown in Fig. 2B, the three electrodes connected through the microfluidic channel tab when the sensor was filled with solution.

2.3. Assembly of AuNPs/PPy/o-μPEIS

The as-purified PPy hydrogel was dried under a vacuum at 70 °C to obtain dehydrated hydrogel. Then, 1 mg dehydrated hydrogel was dispersed ultrasonically in 1 mL 0.05% Nafion solution to obtain a homogeneous suspension. 4.0 μL of prepared suspension was dropped onto the WE and dried naturally. Subsequently, AuNPs were electrodeposited on the as-prepared PPy/o-μPEIS by amperometry via spontaneous reduction of Au^{3+} ions to Au^0 (Hezard et al., 2012). 1.5 mM $HAuCl_4 \cdot 3H_2O$ containing 0.1 M KNO_3 and was electrodeposited on the WE under a given potential of 0.1 V for 200 s. As a control, AuNPs modified o-μPEIS (AuNPs/o-μPEIS) was also prepared using the same method. Finally, we stored AuNPs/PPy/o-PEIS at 4 °C for further use.

2.4. Electrochemical assay of AuNPs/PPy/o-μPEIS

The AuNPs/PPy/o-μPEIS was folded and readied for IL-6 detection. The direct immunoassay method was used in this detection process. 10 uL cAb-magnetic beads (diluted 1: 50) was incubated with 15 uL of different concentrations of IL-6 overnight at 4 °C. After incubation, the mixture was directly pipetted onto the paper surface and washed with PBST three times to remove the unconjugated IL-6. An external magnet was placed on the bottom of the WE to retain the magnetic beads. After that, 30uL dAb (diluted 1:200) was introduced into the system by incubation chamber and incubated with IL-6/cAb-magnetic beads for 60 min at 37 °C, followed by washing with PBST three times. Then, 30 uL avidin-HRP (diluted 1:1000) was incubated with dAb/IL-6/cAb-magnetic beads for 37 min at 37 °C. After thorough rinsing with PBST, only the HRP/dAb/IL-6/cAb-magnetic beads were able to be maintained on the surface of the electrode owing to the magnetic field generated from an external magnet. Eventually, 30 uL of TMB/H_2O_2 mixture was dropped onto the detection chamber. After incubation for 10 min, the electrochemical signal was measured.

2.5. Sensing of IL-6 in human serum samples

The developed AuNPs/PPy/o-μPEIS was utilized to the analysis of IL-6 in patient serum sample. The detection procedures are the same as the above steps. We assayed each serum sample three times (n = 3). For comparison, these samples were also analyzed by the hospital using a cytometric bead array (CBA) via a BD FACSVia flow cytometer.

3. Result and discussion

3.1. Principle of the sensing method

Previous studies showed the integration of antibody-labeled magnetic beads into the immunosensor for enriching the immunomagnetic and amplifying signal, allowing sensitive analyte detection (Min et al., 2018; Valverde et al., 2020). Prior to the introduction of antigen, a

hybrid of AuNPs and PPy hydrogel was integrated to boost the conductivity and sensitivity of the proposed o-μPEIS, the principle of which is illustrated in Fig. 1. Once the sample was injected into the sensing system, in the presence of magnetic-cAb and dAb, a sandwich immunocomplex formed via the immunological discrimination between the antigen and antibody, which was subsequently implemented onto the surface of AuNPs/PPy/o-μPEIS by an external magnet. Streptavidin-HRP was incorporated into this sandwich immunocomplex as an enzyme label via the specific affinity between streptavidin and biotin. Upon addition of TMB/H_2O_2 substrate solution, the labeled HRP triggered a typical catalysis reaction and produced electroactive substrates, TMB_{ox}, resulting in a strong electrochemical signal. The electrochemical response was directly correlated with the quantity of immobilized HRP. Thus, quantitative analysis of IL-6 was indirectly achieved by detecting this enzyme amplified electrochemical signal in the proposed AuNPs/PPy/o-μPEIS.

3.2. Characterization of AuNPs/PPy/o-μPEIS

The gelation mechanism of the PPy hydrogel is illustrated in Fig. S5. As a cross-linker and dopant, phytic acid (PA) interacts with PPy to generate hydrogel by protonation reaction. As a consequence of the ability of each PA molecule to interact with multiple PPy chains, an extremely porous 3D nanostructure is created. The excessive number of phosphorus groups from PA renders the PPy hydrogel hydrophilic. The overall polymerization process began by mixing Py (monomer) with PA (dopant) to form a homogeneous solution, then APS (initiator) was added into the above solution to in situ polymerized PPy hydrogel. During this reaction process, we noticed that the color of the mixed precursor solution changed rapidly from brown (the color of PA) to black (the color of PPy), and the solution gelled within 5 min, indicating that this gelation process is almost instantaneous. The water content of the PPy hydrogel was analyzed to be 92.396% (wt/wt) by thermogravimetry (TGA) (Fig. S6).
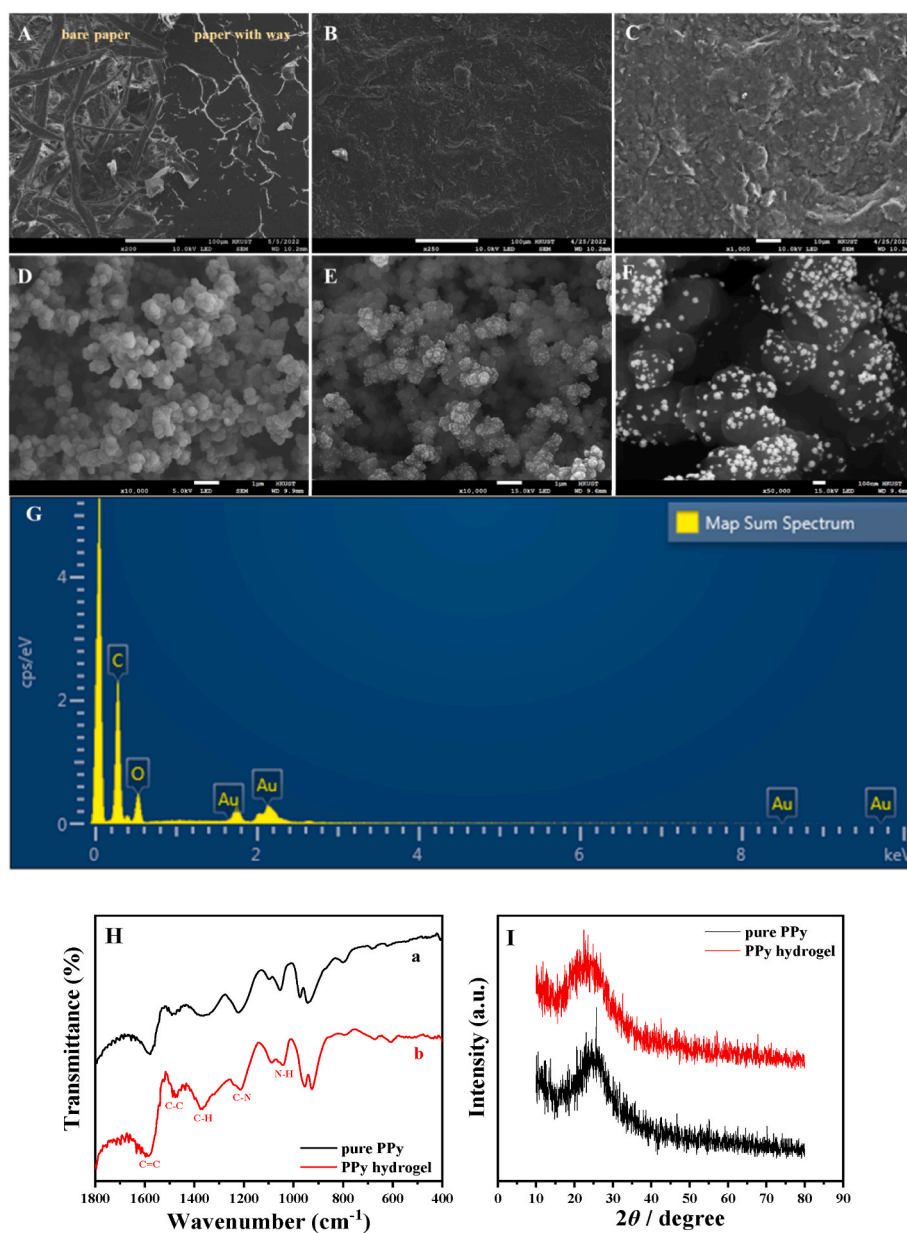
Fig. 3. Characterization of nanostructures: SEM images of (A) the bare paper and paper after wax printing, (B) bare electrode, (C) bare electrode with higher magnification, (D) PPy hydrogel, (E) AuNPs/PPy hydrogel and (F) AuNPs/PPy hydrogel with higher magnification. (G) The EDX map sum spectrum of C, O and Au in AuNPs/PPy hydrogel. (H) FT-IR spectra of the prepared (a) pure PPy and (b) PPy hydrogel. (I) XRD spectra of pure PPy (black curve) and PPy hydrogel (red curve).

An SEM revealed the morphology characterization of the as-prepared PPy hydrogel. First, paper with a porous structure and rough surface was used as the substrate in our immunosensor (Fig. 3A). After wax printing, hydrophilic microfluidic channels for transporting reagents were created (Fig. 3A). Then, carbon ink was printed onto the paper via screen printing to form a WE. The magnified image shows that the carbon ink coated on the cellulose fibers presents as compact and even. Fig. 3B and C demonstrate that the electrode was successfully fabricated on the immunosensor.

Fig. 3D represents the morphology of dehydrated PPy hydrogel with a 3D porous nanostructure consisting of interconnected PPy nanospheres with uniform diameters. Compared to bulk materials, the unique 3D network nanostructure provides a greater surface area for loading electroactive substrates, and the linked pores make it easier for molecules and electrons to diffuse and transport. AuNPs were electrodeposited on the PPy hydrogel consistently, as seen in Fig. 3E. The additional magnified image (Fig. 3F) confirmed that the AuNPs were dispersed on PPy chains densely and homogeneously. The 3D matrix structure of the PPy hydrogel plays a critical part in the high-density loading small size of AuNPs. The loaded AuNPs also increase the active surface area and enhance the electrical conductivity of the electrode, further promoting the performance of our cytokine immunosensor. In Fig. 3G, the element mapping confirms the existence of C, O and Au, giving proof for the characterization of the elemental composition of AuNPs/PPy hydrogel hybrid.

The chemical structure of the AuNPs/PPy hydrogel hybrid was
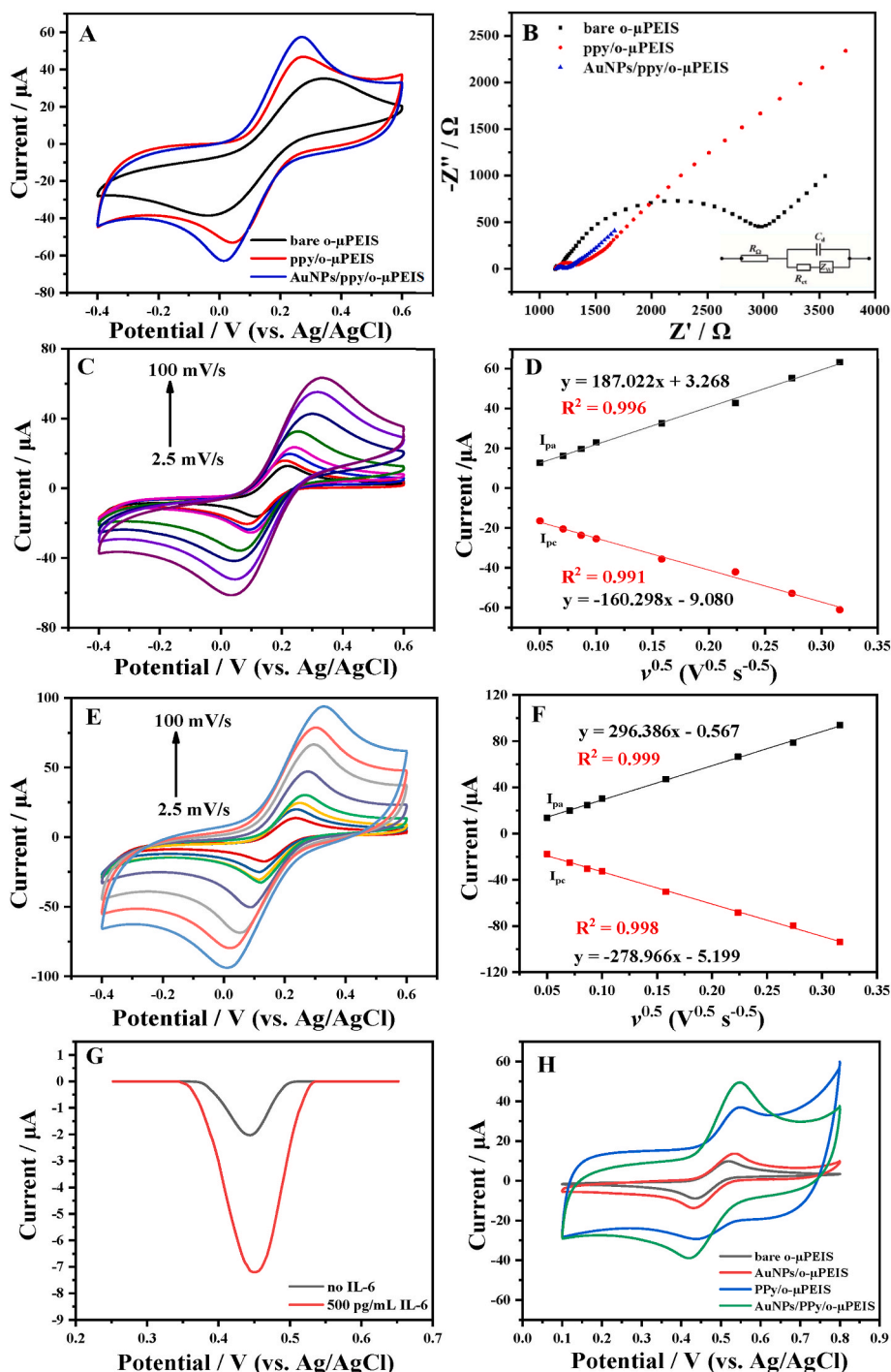
Fig. 4. (A) CV curves for 5 mM $K_3Fe(CN)_6$ containing 0.1 M KCl after each step of the electrode modification procedure. (B) EIS plots of bare o-μPEIS, PPy/o-μPEIS, AuNPs/PPy/o-μPEIS in 5 mM $[Fe(CN)_6]^{3-/4-}$ containing 0.1 M KCl. (Insert: Randel's equivalent circuit). (C) CV curves of bare o-μPEIS in 5 mM $[Fe(CN)_6]^{3-}$ at different scan rates (25–100 mV/s). (D) The linear relationship of peak intensity *vs.* the square root of the scan rate in (C). (E) CV curves of AuNPs/PPy/o-μPEIS in 5 mM $[Fe(CN)_6]^{3-}$ at different scan rates (25–100 mV/s). (F) The linear relationship of peak intensity vs. the square root of the scan rate in (E). (G) The signal response of AuNPs/PPy/o-μPEIS on the absence (black curve) and presence of 500 pg/mL IL-6 (red curve) in 0.01 M PBS. (H) CV curves of bare o-μPEIS, AuNPs/o-μPEIS, PPy/o-μPEIS and AuNPs/PPy/o-μPEIS in the presence of 5 ng/mL IL-6.

characterized by Fourier transform infrared spectroscopy (Fig. 3H). According to the spectra, for curve b, a clear and strong peak at 1577 cm^{-1} belongs to the stretching vibration of C=C in pyrrole rings. Two peaks are obtained at 1488 cm^{-1} and 1375 cm^{-1}, which are assigned to asymmetric stretching vibrations of C–C and C–H bonds in pyrrole rings. The bending vibrations peak of C–N appears at 1220 cm^{-1}. The peaks at 1053 cm^{-1} are attributable to the N–H bonds in-plane deformation vibrations in PPy. These characteristic peaks in the spectra are consistent with the FT-IR spectrum of pure PPy (curve a), implying the successful formation of PPy hydrogel.

The crystalline structure of PPy hydrogel was probed using XRD and is displayed in Fig. 3I. A broad halo appears at $2\theta = 25°$ attributed to the apparent amorphous structure of the conductive polymer. Both diffractograms display similar peaks and are consistent with previous studies reported with PPy (Wang et al., 2020; Zhao et al., 2016). Based on these results, successful synthesis of AuNPs/PPy hydrogel hybrid is entirely demonstrated.

3.3. Electrochemical performance of AuNPs/PPy/o-μPEIS

Cyclic voltammetry (CV) is a valuable and convenient method to describe the fabrication process of this immunosensor. As shown in Fig. 4A, a well-defined pair of symmetric redox peaks, which correspond to Fe(CN)$_6^{3-/4-}$, is discovered on the bare o-μPEIS (black curve). After modifying with PPy hydrogel, an increased peak current is observed for the superior conductivity of PPy hydrogel (red curve). With the further introduction of AuNPs, the redox peak is dramatically augmented (blue curve). This admirable performance benefits from the excellent electrical conductivity and the electron transfer rate of the AuNPs.

Meanwhile, EIS was carried out to investigate the electrochemical performance of the proposed o-μPEIS at different modification stages with a frequency from 1 Hz to 1 MHz at open circuit potential. The diameter of the semicircle at high frequency represents the interfacial electron transfer resistance (R_{et}) of the modified electrode. As shown in Fig. 4B, a large Ret value of ~3000 Ω for bare o-μPEIS (black curve) is observed because of the weak conductivity of the bare electrode. Conversely, after modifying the o-μPEIS with PPy hydrogel, the effective active surface area of the WE was significantly improved, exhibiting a much lower Ret in the spectrum. As AuNPs were coated onto the PPy/o-μPEIS, the resistance reduced further, which provides strong evidence that the electrical conductivity is enhanced. The results of EIS and CV are identical, demonstrating that the cytokine sensing platform was successfully fabricated.

We then evaluated the total effective electroactive surface area (A) of the WE in our proposed immunosensor. CV of bare o-μPEIS and AuNPs/PPy/o-μPEIS was conducted in 5 mM K$_3$Fe(CN)$_6$ at different scan rates (25 to 100 mV/s), as shown in Fig. 4C and E. We can see that the peak current intensity increases with the increase in scan rate. Both oxidation and reduction peaks obey good linear relationships with the square root of the scan rate. According to the Randles−Sevcik equation,

$$I_p = 0.4463nFAC\left(\frac{nFvD}{RT}\right)^{0.5}$$

$$s = \frac{dI_p}{d\sqrt{v}} = 0.4463nFAC\left(\frac{nFD}{RT}\right)^{0.5}$$

$$A = \frac{s}{268600n^{3/2}D^{1/2}C} \qquad (1)$$

where n denotes the number of electrons transferred in a redox system, F (C/mol) is the Faraday constant, C represents the bulk concentration of analyte activity (mol/cm^3), v is scan rate (V/s), D defined as the diffusion coefficient of the analyte (cm^2/s), R denotes the universal gas constant (J/K mol) and T means temperature (K). The average A of bare o-μPEIS and AuNPs/PPy/o-μPEIS were calculated to be 0.047 cm^2 and

0.077 cm^2, respectively. The results show that the electrochemical effective active area increased by 63.8% after modifying AuNPs/PPy hydrogel hybrid, indicating more active sites participated in the electrons transfer on the electrode surface.

Accordingly, the feasibility of the proposed immunosensor for IL-6 detection was investigated. As shown in Fig. 4G, a slight peak appears, which corresponds to the reduction of TMB in the absence of the target. However, when the working solution containing IL-6 flowed into the sensing system, the reduction peak current intensity was significantly enhanced. These satisfactory results of our proposed immunosensor could be attributed to (1) the hybrid of AuNPs and PPy hydrogel amplifying the detection signal of this paper-based immunosensor; (2) the integration of magnetic immunoassays into the paper-based immunosensor enables the signal readout with remarkable amplification in both sensitivity and stability; (3) the HRP grabbed by biotin modified dAb triggers the typical HRP-based catalytic reaction in the presence of TMB/H$_2$O$_2$ substrate, leading to a significantly enhanced electrochemical signal. To demonstrate the merits of the proposed immunosensor, the control experiments were investigated by evaluating the electrochemical response of different sensing platform modification stages to the same target cytokine concentration. As displayed in Fig. 4H, compared to bare o-μPEIS, AuNPs/o-μPEIS and PPy/o-μPEIS, the CV curve of AuNPs/PPy/o-μPEIS provides a more significant reduction in peak current, which is attributable to the reduction of TMB$_{ox}$ generated by HRP catalyzed TMB/H$_2$O$_2$ substrate, demonstrating that the hybrid of AuNPs and PPy hydrogel had a synergistic amplifying impact on the electron transfer.

3.4. Analytical performances of the AuNPs/PPy/o-μPEIS

Under optimal conditions (Fig. S7), the electrochemical performance of as-prepared AuNPs/PPy/o-μPEIS for IL-6 analysis was further investigated. Logically, the incremental IL-6 brings in more HRP, which catalyzes more TMB in the presence of H$_2$O$_2$, exhibiting higher DPV current. In Fig. 5A, the DPV signal outputs positively correlate with the target concentration. The obtained results match with the detection mechanism of the proposed immunosensor. Fig. 5B indicates the DPV current intensity increase linearly as the logarithm of IL-6 concentration, ranging from 5 to 1000 pg/mL. The mathematical expression was calculated to be $\triangle I = 2.366\log (C_{IL-6}) - 1.267$ (R = 0.992), where $\triangle I$ is the difference in DPV peak intensity of various targets and blank. The detection limit was defined as 0.654 pg/mL with a sensitivity of 30.73 μA (pg/mL)$^{-1}$ cm^{-2} based on 3 × the standard deviation of the blank sample divided by the slope of the calibration curve. According to the information, the level of IL-6 in serum is typically higher than 11.6 pg/mL in individuals who suffered moderate/critical ill (Kwon et al., 2020), indicating the tremendous potential for clinical applications in detecting IL-6 in COVID-19-infected individuals. In comparison to other electrochemical immunosensors for detecting IL-6 in reported works, our proposed immunosensor possesses a relatively lower LOD with a wider dynamic range (Table S1). In addition, we also compared our electrochemical immunosensor with other sensors, the results in Table S2 also indicate the superiority of our immunosensor in the detection of IL-6.

3.5. Evaluation of selectivity and reproducibility

The selectivity of the proposed paper-based immunosensor to IL-6 was investigated in the presence of several common proteins in the human body (IL-8, IL-10, CCL-2, CCL-5, tnf-a), whose concentrations were higher (10-fold) than that of the IL-6 (50 pg/mL). As displayed in Fig. 5C, the DPV current signal shows a slight change when these interferents are present, suggesting the superior selectivity of the proposed immunosensor to IL-6.

For sensing devices, especially for this cheap, disposable, paper-based device, stability and repeatability are essential for assessing the capacity of an immuno-device in practical applications. The constructed
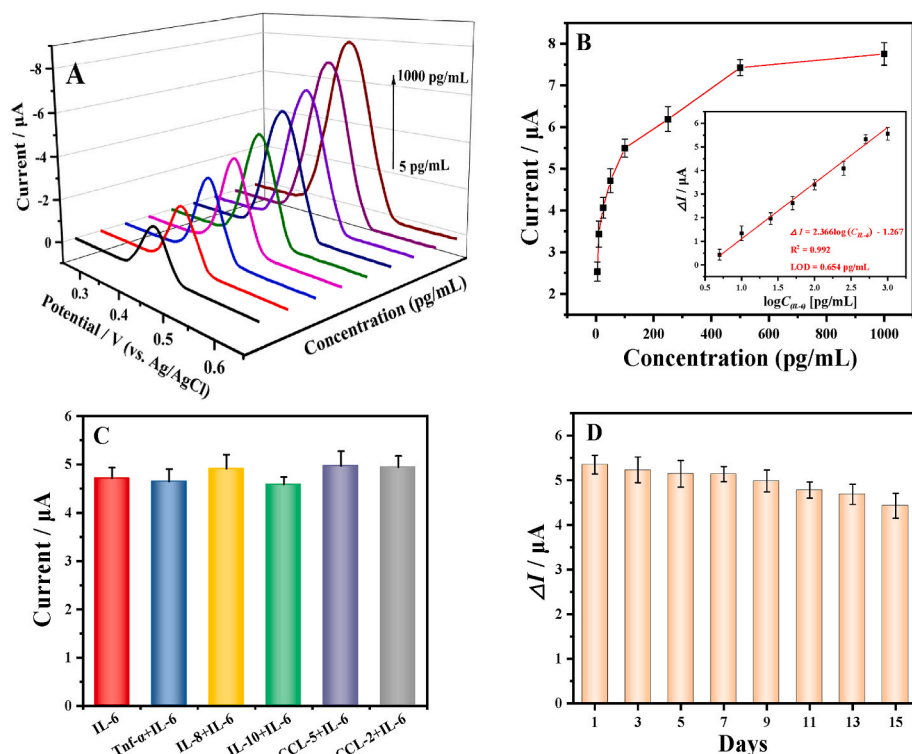
Fig. 5. (A) DPV currents of different concentrations of IL-6 (5, 10, 25, 50, 100, 250, 500, 1000 pg/mL) on the proposed AuNPs/PPy/o-µPEIS in 0.01 M PBS. (B) Calibration curve of the DPV current responses *vs.* the concentration of IL-6. Insert: fitted linearity curve the peak current *vs.* the logarithm of IL-6 concentrations in the range of 5 to 1000 pg/mL. The sensitivity is 30.73 µA (pg/mL)$^{-1}$ cm^{-2}.(C) Evaluation of the selectivity of AuNPs/PPy/o-µPEIS for detecting IL-6 in the presence of different interferents (IL-8, IL-10, CCL-2, CCL-5, tnf-a). The concentration of IL-6 is 50 pg/mL. The specificity is 96.26%. (D) Stability assessment of AuNPs/PPy/o-µPEIS in 500 pg/mL IL-6 after stored for 1d, 3d, 5d, 7d,11d,13d and 15d.

electrodes were stored in N_2 atmosphere and tested for 15 consecutive days. IL-6 of 500 pg/mL was used for the assessment. As displayed in Fig. 5D, the signal obtained by DPV mode decreased by 12.25% after 15 days of storage. The results show our proposed immunosensor has acceptable stability. In addition, six individual AuNPs/PPy/o-µPEIS were constructed in the same batch to detect the same concentration of IL-6 (500 pg/mL). Fig. S8 shows the results of six parallel experiments, demonstrating good repeatability of the proposed paper-based immunosensor.

3.6. Real sample detection

The capability of clinical detection was verified by assaying five different patients' serum samples obtained from Prince of Wales Hospital. These samples were also measured by cytometric bead array (CBA) via a BD FACSVia flow cytometer, which was used as a reference method in the hospital. Under optimal conditions, serum samples with known levels of IL-6 ranging from 9.26 to 92.64 pg/mL were detected directly by our proposed immunosensor. The results were compared with the reference results and these are summarized in Table 1. It was calculated that the relative errors between the reference method and our method were between -7.76% and 10.7%. The accuracy is 93.94%. These results thus indicate that our proposed AuNPs/PPy/o-µPEIS holds great promise for clinical application.

4. Conclusion

This work demonstrated for the first time a novel AuNPs/PPy hydrogel hybrid modified origami microfluidic paper-based electrochemical immunosensor to detect cytokine. Integration of AuNP/PPy hydrogel hybrid into paper based immunosensor enabled the improvement of sensitivity and enlargement of the detection range due to the superior properties of this hybrid materials, including admirable electroconductivity, good biocompatibility and a larger effective surface area. More importantly, this proposed AuNPs/PPy/o-µPEIS is universally applicable to various proteins detection and its manufacturing cost

Table 1
Comparison of the results of IL-6 in patients' serum by our proposed immunosensor and reference value. (n = 3). The accuracy is 93.94%.

Sample	Reference (pg/mL)	Measured (pg/mL± sd)	Relative Errors (%)
1	9.26	8.55 ± 0.13	−7.67
2	12.49	12.34 ± 0.11	−1.20
3	23.71	22.32 ± 0.19	−5.86
4	42.79	47.37 ± 0.26	10.70
5	71.95	66.58 ± 0.21	−7.46
6	92.64	85.45 ± 0.25	−7.76
7	104.03	105.88 ± 0.14	1.80
8	160	169.63 ± 0.28	6.01

per test is under 0.428 USD. Our proposed immunosensor demonstrates superior sensing performance for the detection of IL-6, providing a lower LOD of 0.654 pg/mL, thus satisfying the criteria for biomedical analysis. We envision this origami microfluidic paper-based device to become a promising tool for predicting the health status of COVID-19 patients.

CRediT authorship contribution statement

Dongmin Shi: conceived the project, conducted the experiments and wrote the manuscript. **Chiye Zhang:** analyzed and processed the data. **Xiaoyuan Li:** coordinated the overall research. All authors revised the article and gave their approval for publication. **Jie Yuan:** coordinated the overall research, All authors revised the article and gave their approval for publication, and.

Declaration of competing interest

The authors declare that they have no known competing financial interests or personal relationships that could have appeared to influence the work reported in this paper.

Data availability

Data will be made available on request.

Acknowledgement

Appendix A. Supplementary data

Supplementary data to this article can be found online at https://doi.org/10.1016/j.bios.2022.114898.

References

Andersen, K.G., Rambaut, A., Lipkin, W.I., Holmes, E.C., Garry, R.F., 2020. Nat. Med. 26 (4), 450–452.

Broughton, J.P., Deng, X., Yu, G., Fasching, C.L., Servellita, V., Singh, J., Miao, X., Streithorst, J.A., Granados, A., Sotomayor-Gonzalez, A., Zorn, K., Gopez, A., Hsu, E., Gu, W., Miller, S., Pan, C., Guevara, H., Wadford, D.A., Chen, J.S., Chiu, C.Y., 2020. Nat. Biotechnol. 38 (7), 870–874.

Cazzolla, A.P., Lovero, R., Lo Muzio, L., Testa, N.F., Schirinzi, A., Palmieri, G., Pozzessere, P., Procacci, V., Di Comite, M., Ciavarella, D., Pepe, M., De Ruvo, C., Crincoli, V., Di Serio, F., Santacroce, L., 2020. ACS Chem. Neurosci. 11 (17), 2774–2781.

Chen, G., Wu, D., Guo, W., Cao, Y., Huang, D., Wang, H., Wang, T., Zhang, X., Chen, H., Yu, H.J., Zhang, X., Zhang, M., Wu, S.J., Song, J., Chen, T., Han, M., Li, S., Luo, X., Zhao, J., Ning, Q., 2020. J. Clin. Investig. 130 (5), 2620–2629.

de Lima, L.F., Ferreira, A.L., Torres, M.D.T., de Araujo, W.R., de la Fuente-Nunez, C., 2021. Proc. Natl. Acad. Sci. USA 118 (30), e2106724118.

Gao, Z., Song, Y., Hsiao, T.Y., He, J., Wang, C., Shen, J., MacLachlan, A., Dai, S., Singer, B.H., Kurabayashi, K., Chen, P., 2021. ACS Nano 15 (11), 18023–18036.

Hezard, T., Fajerwerg, K., Evrard, D., Collière, V., Behra, P., Gros, P., 2012. J. Electroanal. Chem. 664, 46–52.

Indalao, I.L., Sawabuchi, T., Takahashi, E., Kido, H., 2017. Arch. Virol. 162 (1), 201–211.

Kwon, J.-S., Kim, J.Y., Kim, M.-C., Park, S.Y., Kim, B.-N., Bae, S., Cha, H.H., Jung, J., Kim, M.-J., Lee, M.J., Choi, S.-H., Chung, J.-W., Shin, E.-C., Kim, S.-H., 2020. Am. J. Trop. Med. 103 (6), 2412–2418.

Li, L., Wang, Y., Pan, L., Shi, Y., Cheng, W., Shi, Y., Yu, G., 2015. Nano Lett. 15 (2), 1146–1151.

Liang, J., Zhang, J., Wu, C., Hu, X., Lu, Y., Wang, G., Yu, F., Zhang, X., Wang, Y., 2020. Biosens. Bioelectron. 155, 112105.

Martinez, A.W., Phillips, S.T., Butte, M.J., Whitesides, G.M., 2007. Angew. Chem. Int. Ed. 46 (8), 1318–1320.

Maucourant, C., Filipovic, I., Ponzetta, A., Aleman, S., Cornillet, M., Hertwig, L., Strunz, B., Lentini, A., Reinius, B., Brownlie, D., Cuapio, A., Ask Eivind, H., Hull Ryan, M., Haroun-Izquierdo, A., Schaffer, M., Klingström, J., Folkesson, E., Buggert, M., Sandberg Johan, K., Eriksson Lars, I., Rooyackers, O., Ljunggren, H.-G., Malmberg, K.-J., Michaëlsson, J., Marquardt, N., Hammer, Q., Strålin, K., Björkström Niklas, K., null, n., 2020. Sci. Immunol. 5 (50), eabd6832.

Min, J., Nothing, M., Coble, B., Zheng, H., Park, J.H., Im, H., Weber, G.F., Castro, C.M., Swirski, F.K., Weissleder, R., Lee, H., 2018. ACS Nano 12 (4), 3378–3384.

Mou, L., Jiang, X., 2017. Adv. Healthc. Mater. 6 (15), 1601403.

Naseri, M., Simon, G.P., Batchelor, W., 2020. Anal. Chem. 92 (10), 7307–7316.

Nge, P.N., Rogers, C.I., Woolley, A.T., 2013. Chem. Rev. 113 (4), 2550–2583.

Noh, S., Lee, H., Kim, J., Jang, H., An, J., Park, C., Lee, M.H., Lee, T., 2022. Biosens. Bioelectron. 207, 114159.

Peng, J., Guan, J., Yao, H., Jin, X., 2016. Anal. Biochem. 492, 63–68.

Peppard, J.V., Rediske, J.J., Koehler, J.A., Koehne, C.F., 1992. J. Immunol. Methods 148 (1), 23–28.

Qi, J., Li, B., Wang, X., Fu, L., Luo, L., Chen, L., 2018. Anal. Chem. 90 (20), 11827–11834.

Santhiago, M., Wydallis, J.B., Kubota, L.T., Henry, C.S., 2013. Anal. Chem. 85 (10), 5233–5239.

Song, Y., Lin, B., Tian, T., Xu, X., Wang, W., Ruan, Q., Guo, J., Zhu, Z., Yang, C., 2019. Anal. Chem. 91 (1), 388–404.

Stenken, J.A., Poschenrieder, A.J., 2015. Anal. Chim. Acta 853, 95–115.

Tanaka, T., Narazaki, M., Kishimoto, T., 2014. Cold Spring Harbor Perspect. Biol. 6 (10).

Tenda, K., van Gerven, B., Arts, R., Hiruta, Y., Merkx, M., Citterio, D., 2018. Angew. Chem. Int. Ed. 57 (47), 15369–15373.

Tetro, J.A., 2020. Microb. Infect. 22 (2), 72–73.

Toma, M., Tawa, K., 2016. ACS Appl. Mater. Interfaces 8 (34), 22032–22038.

Torrente-Rodríguez, R.M., Lukas, H., Tu, J., Min, J., Yang, Y., Xu, C., Rossiter, H.B., Gao, W., 2020. Matter 3 (6), 1981–1998.

Torres, M.D.T., de Araujo, W.R., de Lima, L.F., Ferreira, A.L., de la Fuente-Nunez, C., 2021. Matter 4 (7), 2403–2416.

Valverde, A., Serafín, V., Garoz, J., Montero-Calle, A., González-Cortés, A., Arenas, M., Camps, J., Barderas, R., Yáñez-Sedeño, P., Campuzano, S., Pingarrón, J.M., 2020. Sensor. Actuator. B Chem. 314, 128096.

Wang, M., Cui, M., Liu, W., Liu, X., 2019. J. Electroanal. Chem. 832, 174–181.

Wang, Y., Ma, W., Guo, L., Song, X., Tao, X., Guo, L., Fan, H., Liu, Z., Zhu, Y., Wei, X., 2020. J. Mater. Sci. Mater. Electron. 31 (8), 6263–6273.

Wu, F., Zhao, S., Yu, B., Chen, Y., Wang, W., Song, Z., Hu, Y., Tao, Z., Tian, J., Pei, Y., Yuan, M., Zhang, Y., Dai, F., Liu, Y., Wang, Q., Zheng, J., Xu, L., Holmes, E.C., Zhang, Y., 2020. Nature 579 (7798), 265–269.

Yang, M., Ren, X., Yang, T., Xu, C., Ye, Y., Sun, Z., Kong, L., Wang, B., Luo, Z., 2021. Chem. Eng. J. 418, 129483.

Yang, X., Yu, Y., Xu, J., Shu, H., Xia, J.a., Liu, H., Wu, Y., Zhang, L., Yu, Z., Fang, M., Yu, T., Wang, Y., Pan, S., Zou, X., Yuan, S., Shang, Y., 2020. Lancet Respir. Med. 8 (5), 475–481.

Zhai, D., Liu, B., Shi, Y., Pan, L., Wang, Y., Li, W., Zhang, R., Yu, G., 2013. ACS Nano 7 (4), 3540–3546.

Zhang, T., Deng, R., Wang, Y., Wu, C., Zhang, K., Wang, C., Gong, N., Ledesma-Amaro, R., Teng, X., Yang, C., Xue, T., Zhang, Y., Hu, Y., He, Q., Li, W., Li, J., 2022. Nat. Biomed. Eng. 6 (8), 957–967.

Zhao, J., Wu, J., Li, B., Du, W., Huang, Q., Zheng, M., Xue, H., Pang, H., 2016. Prog. Nat. Sci. 26 (3), 237–242.